Non-linear optical properties of β-D-fructopyranose calcium chloride MOFs: an experimental and theoretical approach

Non Linear Optical Properties of β-D-Fructopyranose Calcium Chloride MOFs: an Experimental and Theoretical Approach

DOMENICA MARABELLO* [a,b], PAOLA ANTONIOTTI[a], PAOLA BENZI[a,b], CARLO CANEPA[a], ELIANO DIANA[a,b], LORENZA OPERTI[a,b]

[a] *Dipartimento di Chimica, University of Torino, Italy*

[b] *CrisDi-Interdepartmental Center for Crystallography, University of Torino, Italy*

E-mail: domenica.marabello@unito.it, +390116707505

LEONARDO MORTATI[c], MARIA PAOLA SASSI[c]

[c] *INRIM – Istituto Nazionale di Ricerca Metrologica, Italy*

Abstract: The second harmonic generation (SHG) properties of two MOFs, obtained from fructose and calcium chloride, were studied using a Non Linear Optics Multimodal microscope. The first-order hyperpolarizability and the second-order susceptibility were calculated at the DFT level of theory. Moreover, a semi-classical approach to non-linearities in the optical behaviour was used in order to determine the features responsible for the SHG. The MOFs were synthesized both in ethanol and by solid-solid interaction, with a simple, rapid, and low-cost methodology with no environmental impact, and were characterized with IR and RAMAN spectroscopy and both single-crystal and powder X-ray diffraction. Both the metal-carbohydrate based MOFs show an interesting SHG intensity: in particular, compound **1** shows an average SH intensity more than twice that of sucrose, in agreement with the theoretical results. A favorable combination of optical properties, transparency, thermal and chemical stability makes compound **1** a potential candidate for applications in electro-optics devices.

Keywords: Second Harmonic Generation; non-linear optic; Metal Organic Framework; X-ray diffraction; second-order susceptibility

1. Introduction

Metal Organic Frameworks (MOFs), being generally solid crystalline materials, represent an ideal category of compounds to design functional materials with physical properties dependent on crystal symmetry. In particular, the second harmonic generation (SHG) property is strongly dependent on the absence of the inversion centre in the crystal structure [1]. Furthermore, in a non-centrosymmetric MOF, the presence of asymmetric ligands can introduce an additional electronic asymmetry and high hyperpolarizability, that seems to be strictly related to the SHG intensity [2]. Materials, capable of an efficient conversion of frequency from IR to UV-VIS, are of great interest for many applications such optical communication systems, laser sensors, optical hard disks, spectroscopical or medicinal lasers and also for biological and medical applications as, for example, imaging agents and delivery vehicles for therapeutic agents [3]. The main requirements for a material to be successfully utilized for those applications are: non-zero non-linear optical coefficient (guaranteed by the absence of the inversion centre), transparency at all the wavelengths involved, efficient energy transfer between the optical waves propagating through the crystal, good physical properties (low vapour pressure and high hardness) and good optical properties, such as stability under an IR laser radiation, large birefringence, and low dispersion. Moreover, for biological applications non-toxic and bio-compatible properties are required. Carbohydrates can be considered good building units for MOFs with those applications, because they are low-cost and bio-compatible chiral materials. The SHG efficiency of many mono-, di- and tri-saccharides have been examined [4], and a correlation between their crystal systems and

SHG efficiencies has been evidenced: saccharides with large SHG efficiencies crystallize in the crystal systems with lower symmetry, such as the monoclinic rather than the orthorhombic. Due to the presence of several OH groups that can coordinate metal ions, carbohydrates represent good asymmetric poly-dentate ligands for the formation of MOFs. Complexation of a metal with asymmetric organic ligands generally leads to solid materials with low symmetry, that could show interesting second-order non-linear optics (NLO) properties.
Since calcium compounds participate in a variety of biological processes, playing important roles such as calcium storage, calcification and calcium-dependent interactions in cells, calcium is one of the most studied alkaline-earth metals that can bind carbohydrates [5]. However, relatively few complexes of neutral carbohydrates with calcium ion have been isolated and characterized [6]. In this work we report, for the first time, a theoretical and experimental study on Non Linear Optical properties of MOFs obtained from fructose and calcium chloride, $[Ca(C_6H_{12}O_6)(H_2O)_2]Cl_2$ (**1**) and $[Ca(C_6H_{12}O_6)_2(H_2O)_2]Cl_2{\cdot}H_2O$ (**2**). The X-ray structures of compounds **1** and **2** were determined for the first time by Craig *et al*. in 1974 [6g,h] and their structures have only been briefly described: no information about MOF building is referenced. Both structures were re-determined in this work in order to obtain best quality data. We have measured by SHG microscopy both their SH intensity and the SH intensity ratio with respect to sucrose. Compounds **1** and **2** have been also studied with DFT theoretical calculations in order to investigate their relative stability. Modelling of simple complexes of fructose with $CaCl_2$ were used to single out which structures gives the highest value of the second-order susceptibility $\chi^{(2)}$. Moreover, in order to determine the features responsible for the SHG, a semi-classical approach to nonlinearities in the optical behavior was used. The complexes investigated in this work have been obtained with a new synthesis methodology, simple, rapid, low-cost and with no environmental impact. The compounds were subsequently characterized with IR and RAMAN spectroscopy and both single-crystal and powder X-ray diffraction.

2. Experimental Section

2.1. Synthesis. D(-)fructose was purchased from Sigma Aldrich, anhydrous CaCl2 93% from Alfa Aesar, and absolute anhydrous ethanol from Carlo Erba. All reagents were used as supplied.
Anhydrous calcium chloride and β-D-fructose were dissolved in 6 cc of ethanol at 348 K in the stoichiometric ratios 3:1, 2:1, 1:1, 1:2. After one hour in the 3:1, 2:1, and 1:1 solutions fructose is completely dissolved while in the 1:2 and 1:3, part of it remains undissolved and was subsequently filtered. The solutions were slowly evaporated at room temperature in glass test-tubes. After a few hours in the 3:1 and 2:1 solutions a gelatinous substance was formed, and after three days this gelatinous substance was completely dissolved and white crystalline powders were deposited on the walls of the test-tubes. The remaining solutions were transferred into closed vials and, after a few days, a great amount of new colourless well-shaped crystals were deposited. These crystals were filtered on paper and dried at room temperature.
For the solid state synthesis, powdered anhydrous calcium chloride and β-D-fructose were dried in an oven at 333 K for one day, mixed in the stoichiometric ratios 3:1, 2:1, 1:1, 1:2, and ground together in an agate mortar inside a dry box, in order to avoid dissolution of the powders due to the hygroscopic behaviour of calcium chloride.
2.2. X-ray diffraction. Single-crystal and powder patterns were collected at room temperature using an Oxford Diffraction Gemini R Ultra diffractometer [7]. The CrysAlisPro [8] package was used for data collection and integration. Crystals suitable for single-crystal X-ray diffraction were selected from the 2:1 and 1:2 solutions for compounds **1** and **2**, respectively. Data have been collected with graphite monocromatized Mo-Kα radiation (0.71073 Å). SHELXS [9] for resolution, SHELXL-2012 [10] for refinement and Olex2 [11] for graphics. Compound **1**: monoclinic, $P2_1$, a=7.0731(2) Å, b=11.7023(3) Å, c=7.7808(3) Å, β=93.998(3)°, Z=2,

7220 reflections measured, 3460 unique (R_{int} = 0.0296) which were used in all calculations. The final $wR(F^2)$ was 0.0711. Compound **2**: monoclinic, C2, a=16.016(1), b=7.8393(2), c=9.2442(3), β=98.601(3)°, Z=2, 5988 reflections measured, 3428 unique (R_{int} = 0.0245) which were used in all calculations. The final $wR(F^2)$ was 0.0734. Further details on crystal data, data collection and refinement are reported in supplementary materials. All but the hydrogen atoms were anisotropically refined. All H atoms have been found on difference Fourier maps, but they have been calculated and refined riding on the bonded atom, with U_{iso}=1.2 or 1.5 U_{eq} of the bonded atom. Crystallographic data have been deposited with the Cambridge Crystallographic Data Centre, CCDC 1023479-1023480.

Each sample for X-ray powder diffraction was prepared by mixing the powder with a little drop of hydrocarbon based oil [12] to obtain a ball of about 0.5 mm and mounted on a glass capillary. Crystals obtained from solutions were not ground in order to avoid degradation. To reduce hygroscopic degradation, the patterns of the samples derived from 3:1 and 2:1 solid state mixtures were recorded in Lindemann glass capillaries. The powder diffraction patterns were collected with mirror monochromatized Cu-Kα radiation [13] (λ=1.5418 Å) and the samples were rotated 30 degrees during data collection in order to limit not-grinding errors on peaks intensity. Maximum resolution 1.4 Å and exposure time 30 s.

2.3. IR, RAMAN spectra. IR spectra of crystalline samples were recorded on a Bruker Vertex 70 spectrophotometer, equipped with an anvil ATR cell. Raman spectra were obtained with a Horiba Jobin Yvon HR800 instrument on a crystalline sample, equipped with an Olimpus BX41 microscope. Samples have been excited with a 633 nm laser radiation with a magnification ratio of 50x. Infrared and Raman vibrational frequencies of compounds **1** and **2** are reported in supplementary materials.

2.4. Second Harmonic Generation Measurements. Both complex **1** and **2** together with sucrose as reference were characterized in terms of second harmonic generation emission, using a Non Linear Optics Multimodal microscope described in another paper [14].

Single crystals of the compounds were mounted in special sample holders and imaged using second harmonic generation microscopy technique. The specimens were excited using a pulsed source of about 5 ps pulse length and a wavelength of 915 nm, generated by an OPO (Levante Emerald, APE Berlin) pumped by a master laser (picoTrain, HighQLaser). The excitation source was focused on the sample using a 20x lens (UPLSAPO 20X NA=0.75, Olympus Europe) and the emitted signal was collected in the forward direction using a 4x lens (UPLSAPO 4X NA=0.16, Olympus Europe), optically filtered allowing only a transmission window in a wavelength range between 420 and 490 nm (D455/70X, Chroma Technology).

Using an optical spectrum analyzer it was verified that compounds generate only second harmonic signal without any other spectral components (Fig. 1), validating the transmission window of the microscope detection system.

Fig. 1

The crystals had a size slightly greater than 100 µm, while the focusing size of the excitation source was in the order of few µm. Using an excitation lens with a numerical aperture of 0.75, the excitation wave vectors could have multiple angles easing the phase matching condition. In order to extract the emission ratios of the different compounds, the crystals were imaged in 3D several times at different excitation intensities. For each sample the single crystal was imaged oriented in four orthogonal angles with respect to the sample holder axis. The excitation intensity was modified rotating the beam horizontal polarization with a half waveplate window, using a motorized stage and then transmitting the beam through a polarizer beamsplitter, allowing only horizontal linear polarization exciting the sample. A very small part of the excitation signal was split with a broadband beamsplitter window and sent to a powermeter (PM30, Thorlabs with sensor S120B, Thorlabs). The analogue output of the powermeter was measured simultaneously with the second harmonic signal generated by the samples.

In each measurement session, samples were imaged using twenty different excitation intensities. Samples were 3D imaged in each orthogonal angle collecting about 15 Z slice images, setting the Z pitch between images in a way to acquire the whole sample.

Using ImageJ software [15], a specific plugins was developed to extract the average second harmonic generated signal and the related average excitation intensity from each slice of the 3D images. Before running the plugin over the set of the collected 3D images an overall max intensity Z projection was performed and the region outside the compound shape was cleared and it was manually chosen a threshold value to discriminate the foreground object from the background. The plugin was then launched using as input parameters the size in pixel units of the smaller object recognizable as foreground (in order to avoid salt and pepper effect filtering resulting objects smaller than that size), the chosen threshold value and the number (20) of excitation intensities used during the imaging measurements. At the end of the plugin it was computed a result table containing all the average intensities per slice images and the overall 3D image average intensities together with the related average excitation intensities.

Since the second harmonic signals measured in function of the excitation power must have a quadratic dependence, the plugin also processes the average intensities per excitation power and extracts the fitting parameter related to the following quadratic function that should represent the hyperpolarizability behaviour of the sample:

$$y = ax^2 + b$$

The parameters *a* and *b* were computed for all the orientation angles and an average value of *a* was extracted for each compound in order to take into account an average behaviour of the crystal's emissions (Fig. 2). At the end the ratios of the *a* parameters referred to sucrose were computed for the three samples.

Fig. 2

2.5. Computational methods. The calculations were performed with the GAUSSIAN09 set of programs [16]. All structures were optimized by gradient-based techniques [17] without any symmetry constraint, at the DFT B3LYP [18] level of theory in conjunction with the 6-31G(d) basis set [19]. The critical points were unambiguously characterized by calculating analytical harmonic vibrational frequencies. Total dipole moments, polarizabilities, and first-order hyperpolarizabilities were calculated at the same level of theory. Binding energies were refined by single-point calculations at the B3LYP/6-311G(2d,2p) level of theory on the optimized geometries.

Molecular volumes were computed by averaging ten different volume calculations on the optimized geometries at the B3LYP/6-31G(d) level of theory with the Gaussian09 options scf=tight, volume=tight, and iop(6/45=500,6/46=1) [20].

3. Results and Discussion

3.1. Optimization of synthesis conditions. In previous works the carbohydrates-metal compounds have been obtained from water or water-ethanol solutions through slow evaporation (a few months). In the presence of water, metal ions are surrounded by coordinating water, and the unionized hydroxyl groups of carbohydrates are weak competitors for metal ion coordination. In fact, complexes with functionalized and deprotonated carbohydrate ligands are more common [21]. For this reason, we attempted to obtain simple carbohydrates-metal complexes from ethanol solutions. The solubility of fructose in ethanol is very low, but fructose is completely dissolved after addition of excess calcium chloride or at least in a 1:1 stoichiometric ratio Ca:fructose. This fact suggests that the calcium ions interact strictly with the fructose molecules already in solution, as demonstrated also by the formation of a gelatinous substance in the 3:1 and 2:1 solutions after a few hours from the mixing of the reagents.

In order to understand the process of formation of the complexes, X-ray powder diffraction (XRPD) patterns of the powders deposited on the walls of the test tubes and of the crystals subsequently deposited in the vials were collected, without grinding the powders to avoid degradation. In fact, if those powders were ground in a mortar, a sticky dough would form and the crystalline signals on powders patterns are completely lost. Two compounds have been identified, compounds **1** and **2**, and their patterns were compared with those calculated from single-crystal X-ray structures of FRUCCA [6h] and FRCPCA [6g], obtained from the CSD database [22] (see supplementary materials). Even if their relative peak intensities differ slightly, due to the small error in intensity collection caused by not grinding the powders, the patterns of compounds **1** and **2** correspond to the FRUCCA and FRCPCA, respectively.

During evaporation of the solutions, compound **1** deposits first at the top of the walls of the test tubes. The crystals deposited into the closed vials show instead the pattern of compound **1** from the 3:1 and 2:1 solutions, the pattern of compound **2** from 1:2 and 1:3 solutions, and a mixture of both compounds from solution 1:1. Due to the different stoichiometric ratios of $CaCl_2$ and fructose in the formula unit (1:1 and 1:2 in compounds **1** and **2** respectively), it is not surprising that compound **1** is obtained from solution with an excess of calcium chloride, while compound **2** is mainly deposited in sugar-rich solutions.; in any case, compound **2** is the more abundant product.

In previous works [6g,h] compound **1** is reported as the most stable, while compound **2** was reported being hygroscopic and unstable under radiation. We observed, on the contrary, that crystals of compound **2** obtained with the synthetic methods reported in this work are less hygroscopic than those of compound **1**, although both show sufficient stability in air and with respect to X-ray and IR radiation to permit all measurements.

Powdered anhydrous calcium chloride and β-D-fructose were also mixed directly in the same stoichiometric ratios of the previous solutions and ground together in an oven at 333 K. After a few minutes the powders became lumpy. While the powders from the 1:1, and 1:2 mixtures are stable in air, those from the 3:1 and 2:1 mixtures show hygroscopic behavior due probably to the unreacted calcium chloride. Fig. 3 reports the XRPD patterns of these mixed powders.

Fig. 3

Surprisingly, in the 3:1 mixture, calcium chloride and sugar do not interact as shown by the XRPD pattern, which is simply the sum of the patterns of the two unreacted reagents. The pattern of the 2:1 mixture is instead an indication that calcium chloride reacts completely with sugar forming a new unidentified compound. The 1:1 mixture shows the presence of both compound **1** and **2**, and the 1:2 mixture contains only compound **2** with an excess of fructose. We can thus conclude that compounds **1** and **2** can easily be obtained through solvent-free synthesis. Furthermore, the presence of an unknown compound in the 2:1 mixture suggests that other interesting crystalline compounds with different physical properties may be synthesized from the same starting reagents.

3.2. Crystal structures. In the asymmetric unit of compound **1**, one calcium ion, one sugar molecule, two independent chloride ions, and two independent water molecules connected to the calcium atom are present. The coordination around the metal ion and atom labeling are shown in Fig. 4a: three fructose and two water molecules are coordinated to the same calcium ion, so that the metal atom is surrounded by a shell composed of 7 oxygen atoms, an unusual coordination number for the calcium ion. Each sugar molecule in the crystal is mono- or bi-chelating toward three calcium ions, involving all its OH groups in dative metal-ligand bonds. A network of calcium ions and sugar molecules forms an infinite plane parallel to (001) (Fig. 4b). Consequently this compound must be described of as a bi-dimensional metal organic framework (2D-MOF).

Fig. 4

In the asymmetric unit of compound **2**, half calcium ion, one sugar molecule, one chloride ion, one water molecule connected to the calcium atom, and one half free water molecule are present. In Fig. 5a both the

coordination of the metal atom and the atom labelling are shown: unlike compound **1**, the calcium ion is surrounded by eight oxygen atoms, six from fructose and two from water molecules, the coordination number 8 being the most common in similar calcium complexes. Each fructose molecule is mono- o bi-chelating toward two calcium ion, and, unlike compound **1**, only three of the OH groups (O(2)H,O(3)H,O(6)H) are involved in coordinating the metal. The OH groups not involved in coordinating metal ions are free to interact with the solvent and, probably for this reason, compound **2** is slightly more soluble than compound **1** and was found at the bottom of the test tubes. Compound **1** is the first to crystallize in all solutions.

Fig. 5

In the structure of compound **2**, two fructose molecules bridge two calcium ions, and an infinite thread of fructose and calcium ions develops in the [010] direction (Fig. 5b). Consequently, this compound has to be thought of as a mono-dimensional metal organic framework (1D-MOF).

In Table 1 are reported the Ca-O bond lengths from the X-ray data for the compounds **1** and **2**. It is noticeable that the Ca-O distances are shorter for complex **1** (2.393 Å av.) with respect to complex **2** (2.465 Å av.), probably because of the lower coordination number that reduces the hindrance around the calcium atom.

Table 1

It is interesting to note that carbohydrate-metal salts systems are known to form isomorphous structures. For example, the isomorphous of compound **1** obtained substituting the bromide ion to the chloride [6i], and the isomorphous of compound **2** with the Sr^{2+} ion in the place of Ca^{2+} [6m] are known. Also, two isostructural compounds of sucrose have been reported [23]. Synthetizing new similar MOFs by changing either the metal ion or the anion could induce a different optical behaviour in the material, *i.e*. a different wave length and intensity of the emitted SH radiation. We could thus in principle customize the material synthetized to the desired optical features.

3.3. Vibrational spectra. The Raman and infrared spectra of compounds **1** and **2** were recorded on crystalline samples (Fig. 6).

Fig. 6

The infrared spectra of compounds **1** and **2** have been already reported and compared with vibrational spectra of D-fructose [24]. An interpretation of the spectra has been offered, mainly based on the intermolecular interactions of O-H···X, C-H···X (X=O, Cl), and on the metal coordination of OH groups. In the ν(OH) region it is difficult to discriminate between the modes of the OH groups of fructose and of water (both coordinated to the metal and lattice water). While compound **1** exhibits two bands in the δ(OH) mode at 1640 and 1599 cm^{-1}, compound **2** shows a single band at 1654 cm^{-1}. This behaviour is consistent with the crystalline structure, of compounds **1** and **2**. In fact, compound **1** has two independent water molecule connected to the metal atom, and compound **2** has only one. A shoulder in the infrared band at 1654 cm^{-1} was detected, possibly relevant to the mode of the lattice water in compound **2**. The C-H vibrational modes are involved in intermolecular interactions, however with weaker interactions with respect to the O-H groups. The ν(CH) modes of crystalline D-fructose have been accurately assigned [25]. Tajmir-Riahi [24] assigned these modes for compounds **1** and **2** only on the basis of infrared spectra. Both the anomeric effect and the intermolecular interactions can in principle influence this spectral region. Raman spectra, due to their sharper bands, allow to discriminate between these effects. The strong 3011 cm^{-1} $\nu_a(CH_2)$ mode of hydroxymethyl group is red-shifted in compound **1** (Fig. 6b) with respect to crystalline D-fructose [25].

We observed that in compound **1**, the C(1)-H bonds are not involved in short contacts, and the $C(1)H_2$ group is opposed to the anomeric OH, while in fructose they are *cis*-oriented (Fig. 7).

Fig. 7

The fructose units in compound **2** exhibit a conformation similar to crystalline fructose, but, with the exception of the $C(1)H_2$ groups, the C-H bonds are not involved in short contacts. Nevertheless, the $\nu_a(CH_2)$ mode of the hydroximethyl group is the only blue-shifted mode with respect to crystalline D-fructose. For this

reason, the main influence on the ν(CH) modes seems to depend on the conformations of the fructose unit. The region between 1500-400 cm^{-1} involves the CH deformation and ring skeletal modes. Tajmir-Riahi [24] reported as general trend a lowering of the frequencies, as consequence of metal-coordination to the fructose. However, a more complex behaviour is found by comparing the infrared and Raman spectra, due both to the modest effect of calcium coordination in this spectral region and the difficulty to individuate a specific diagnostic signal. A well-isolated band in the Raman spectrum of fructose is the CH_2 scissoring mode of the hydroxomethyl group (1470 cm^{-1}) that shifts to 1455 cm^{-1} and 1450 cm^{-1} in compound **1** and **2**, respectively. This shift is attributable to the electronic effect induced by the Ca^{2+} ion on the HO-C(1) group, modulated in compound **1** and **2** by the different coordination of calcium.

3.4. Second Harmonic Generation Analysis. Using the method described in the previous section, the fitting parameters *a* and *b* were computed for each compound and the four orientation angles. In Table 2 are reported the average parameters *a* for each orientation angle and their variability for the measurement pairs considering both measurements having a uniform distribution.

Table 2

This leads to the following relation of the associated uncertainty due the repeatability of the measurement pairs:

$$u(a) = \left(\frac{max - min}{2\sqrt{3}}\right) \quad (1)$$

At the bottom of each nested table are showed the overall average of *a* and the average of all the computed uncertainties, in a way to express the overall average variability associated to the average parameter *a*. The parameters *a* differ between each other at the different orientation angles which is theoretically consistent. The parameter *b* were reported for completeness even if they express only a sort of offset between the curves that is useless in order to derive the ratios of the SHG intensities. The ratio of the average parameters *a* related to each compound gives a representation of the ratio of the SHG intensities.

Considering the overall average uncertainty associated to the average parameters *a,* it is computed the uncertainty related to the ratio. This uncertainty takes into account only the average variability associated with the repeatability of the different measurement pairs.

The uncertainty value $u(a_x/a_{sucr})$ is derived using the propagation of the uncertainty:

$$u(a_x/a_{sucr}) = \sqrt{\left(\frac{u(a_x)}{a_{sucr}}\right)^2 + \left(-\frac{u(a_{sucr})a_x}{a_{sucr}^2}\right)^2} \quad (2)$$

A deeper understanding of the overall uncertainty should also take into account other uncertainty sources related to the measurement method such as the detector linearity and noise, the threshold level choice during the image processing, the errors associated to the fitting procedure, the unwanted movements of the sample during the measurement, etc. This will be addressed in future works.

In this case the purpose of the uncertainty is to identify the range associated with the average evaluation variability of the parameter *a* related with the measurement repeatability.

In Table 3 are reported the obtained ratios I/I_{sucr} for the two compounds.

Table 3

Experimentally, compound **1** showed an average SH intensity more than the double of that of sucrose, while compound **2** showed an average SH intensity slightly less than the half of that of sucrose, the SH of compound **1** being about five times more intense with respect to compound **2**. These results can be defined in accordance with the ones computed theoretically, as it is discussed in the next paragraph.

3.5. Computational results. The geometries of compounds **1** and **2** were obtained by optimizing the coordinates of two crystal fragments from the X-ray structures, shown in Fig.s 4b and 5b. Each fragment is formed by three calcium ions, six fructose molecules, six water molecules, and six chloride ions. For sucrose and fructose, units of 3 sucrose molecules and 7 fructose molecules selected from the crystal structures were respectively used as models of the bulk. These geometries were re-optimized at the B3LYP/6-31G(d) level of theory to obtain the corresponding minima.

The optimized structural parameters given in Table 1 show deviations in the computed geometric parameters from the corresponding X-ray data, probably due to the intermolecular interactions in the crystalline state. The maximum difference between the calculated and experimental bond lengths in compound **1** is observed for Ca(1)-O(1W), Ca(1)-O(6), Ca(1)-O(5) bond lengths, and it does not exceed 0.13 Å. The deviation for the other Ca-O bonds is lower than 0.09 Å. For compound **2**, the differences in bond length do not exceed 0.1 Å, and was observed for Ca(1)-O(1W) and Ca(1)-O(3). The deviation for the other Ca-O bonds is lower than 0.05 Å.

One of the most important aspects of ion complexation is ion selectivity, which is considered in terms of the more or less favorable binding energies. The binding energy (BE) is defined as the difference between the energy of the complex and the sum of the energy of the free ligand and free ion: $BE = E_{complex} - (E_{ion} + E_{ligand})$. We evaluated and compared the binding energy of the complexes reported in Fig. 4a (complex **1**) and 5a (complex **2**) in which the Ca^{2+} ions show a different coordination. The calculated binding energy for complex **1** (-313.4 kcal mol^{-1}) is smaller than that for complex **2** (-353.3 kcal mol^{-1}). Thus we can conclude that complex **2** is more stable than complex **1**, according to the fact that complex **2** is more abundant in the products obtained from the solutions. Undoubtedly, the coordination number plays a role in the stabilization of the complex and in fact the usual coordination number in the calcium complexes is eight as in complex **2**.

Density functional theory (DFT) was also used to calculate the dipole moment μ, mean polarizability $< \alpha >$, first static hyperpolarizability β, and molecular volumes. The computational determination of dipole moments, electric polarizability and hyperpolarizability is fundamental to the study of NLO effects and intermolecular interactions. These computed quantities, when obtained with a consistent level of theory and basis set, may be safely compared even in the absence of experimental data. The total dipole moments and the mean polarizabilities in a Cartesian frame are defined as:

$$\mu = \left(\mu_x^2 + \mu_y^2 + \mu_z^2\right)^{1/2} \quad (3)$$

$$< \alpha >= (1/3)\left(\alpha_{xx} + \alpha_{yy} + \alpha_{zz}\right). \quad (4)$$

The total intrinsic hyperpolarizability β_{tot} is defined as

$$\beta_{tot} = \left(\beta_x^2 + \beta_y^2 + \beta_z^2\right)^{1/2}, \quad (5)$$

where $\beta_x = \beta_{xxx} + \beta_{xyy} + \beta_{xzz}$, $\beta_y = \beta_{yyy} + \beta_{yzz} + \beta_{yxx}$, and $\beta_z = \beta_{zzz} + \beta_{zxx} + \beta_{zyy}$ [26].

Table 4 reports the computed μ, $< \alpha >$, and all β components of compounds **1**, **2** and the units of 3 sucrose molecules and 7 fructose molecules.

Table 4

The ratio of SH intensity $\mathrm{I_{fructose}/I_{sucrose}} = 0.02$ was measured experimentally by Perry *et al.* [27]. This sections aims at determining the features responsible for the SHG in compounds **1** and **2** first by using the semi-classical approach to non-linearities in the optical behavior, and second by modelling simple complexes of fructose with $CaCl_2$ to single out which structures give the highest value of the second-order susceptibility

$\chi^{(2)}$. The second-order susceptibility was computed from the total hyperpolarizability given by Eq. (5) using the relation

$$\chi^{(2)} = \beta_{tot}/\varepsilon_0 V \qquad (6)$$

where V is the molecular volume. The driven solution of the Lorentz oscillator gives the atomic electric susceptibility

$$\chi_a = \frac{e^2}{\varepsilon_0 m} \frac{\omega_0^2 - \omega^2}{(\omega_0^2 - \omega^2)^2 + (\gamma\omega)^2} \qquad (7)$$

for a single resonant angular frequency ω_0 and a driving angular frequency ω. In Eq. (7) e and m are the electron charge and mass, respectively. The friction parameter γ will be treated as a free parameter. The Lorentz-Lorenz relation

$$n^2 = \frac{1 + \frac{2}{3} N\chi_a}{1 - \frac{1}{3} N\chi_a}, \qquad (8)$$

strictly valid for cubic crystals with a number density of oscillator N, will be used to estimate the indexes of refraction n at both the fundamental and SH frequency, which will in turn be used in the expression for the intensity of the SH at coherence length

$$I_{2\omega} = 2\left(\frac{\mu_0}{\varepsilon_0}\right)^{1/2} \frac{\left(\chi^{(2)}\right)^2}{n_{2\omega} n_\omega^2 (n_\omega - n_{2\omega})^2} I_\omega^2 \sin^2\left(\frac{\Delta k L}{2}\right). \qquad (9)$$

Since the random orientation of the crystal with respect to the driving electric field does not allow for phase matching, the factor $\sin^2(\Delta kL/2)$ in Eq. (9) is taken equal to unity, and the SHG is assumed limited within the coherence length. The SH intensities versus the ratio ω/ω_{exc} for compounds **1**, **2**, sucrose, and fructose are plotted in Fig. 8.

Fig. 8

The intensities exhibit two resonant peaks at angular frequencies that make the difference $n_\omega - n_{2\omega}$ in the denominator of Eq. (9) equal to zero.

Figure 8 also reports (at arbitrary values of the ordinate) the resonant frequencies ω_0 for the four compounds under investigation, estimated from the HOMO-LUMO energy difference. Higher values of ω_0 place the resonant peaks at higher frequencies, so that the peaks of SH intensity for different compounds follow the same order as the resonant frequencies. The value of γ was chosen to match the computed and measured ratio of SH intensity between compound **1** and sucrose at frequency ω_{exc}, and kept constant in all subsequent calculations. The ratios of SH intensities to sucrose are listed in Table 5 and fit reasonably well to the corresponding measured values (table 3).

Table 5

The value of the SH intensity is thus mainly determined by the factor $n_\omega - n_{2\omega}$ at the excitation angular frequency ω_{exc}, in turn dependent on the resonant frequency through the term $\omega_0^2 - \omega^2$. Of course the second-order susceptibility $\chi^{(2)}$ also plays a role, appearing as a square in Eq. (9).

We finally address the role of $CaCl_2$ in the enhancement of the intensity of the second harmonic exhibited by the compounds **1** and **2** with respect to pure fructose. The hyperpolarizability and second-order susceptibility of complexes of two fructose molecules and one $CaCl_2$ unit were computed at the B3LYP/6-31G(d) level of theory for the two configurations reported in Fig. 9.

Fig. 9

In configuration **3** the Ca-Cl distances (2.702, 2.660 Å) are similar to the undissociated $CaCl_2$ structure (2.539 Å), while in **4** the distances are comparable to the structure of **1**. The computed second-order susceptibility of structure **3** and **4** (1.18 and 3.72 pm V^{-1}, respectively) suggests that the dissociation of $CaCl_2$ induced by fructose plays a role in the increase of the intensity of the second harmonic emitted by these compounds.

4. Conclusions

This work aims to rationalize the connection between the SHG property and the structural features of two MOFs based on fructose and calcium chloride. It was demonstrated that the coordination of fructose on the calcium ion causes an improvement of the SH intensity with respect to the fructose itself, because of the induced lowering of symmetry and the dissociation of $CaCl_2$ by fructose.
The theoretical calculations on the I/Isucr ratios for the two compounds suggests that, at the excitation angular frequency, the SH intensity is influenced by both the resonant frequency and the second-order susceptibility.
The metal-carbohydrate based MOFs analyzed in this work show a favorable combination of thermal and chemical stability, transparency, and second-order optical nonlinearity; in particular compound **1** shows an interesting SH intensity, and is thus potential candidate for applications in electro-optics devices.
The presence in literature of several isomorphous compounds of these systems suggests the possibility of designing new materials with the desired optical features, i.e. different wave-length regions and intensities of the emitted SH radiation. Furthermore, the remarkable difference in the SH intensity of the two compounds studied, suggests that this property could be “controlled” both by tuning the composition of the system and by the disposition of the MOF’s building units in the crystal. This matter will be the subject for future studies.

Acknowledgements

The authors thank the University of Torino and the Italian Ministero dell’Università e della Ricerca (MiUR) for financial support. This work was partially supported by Joint Research Project SIB54 “Bio-SITrace”, co-funded by European Metrology Research Programme (EMRP). The EMRP is jointly funded by the EMRP participating countries within the EURAMET and the European Union. We thank also the Interdepartmental Centre Scansetti for the opportunity to use the Horiba JobinYvon micro-Raman instrumentation.

References

[1] Chemla D. S., Zyss J. (1987) Non linear optical properties of organic molecules and crystals. Academic Press: New York, 1:2

[2] Evans O. R., Lin W. (2002) Crystal Engineering of NLO Materials Based on Metal−Organic Coordination Networks. Acc. Chem. Res. 35: 511-522

[3] Liang P., Xia W-X., Tian W-M., Yin X-H. (2013) Synthesis, Structures and Properties of Two Metal-Organic Coordination Polymers Derived from Manganese(II), Thiabendazole and Polydentate Carboxylic Acids. Molecules 18: 14826-14839

[4] Bournill G., Mansour K., Perry K. J., Khundkar L., Sleva E. T., Kern R., Perry J. W. (1993) Powder second harmonic generation efficiencies of saccharide materials. Chem. Mater. 5: 802-808

[5] Whitfield, Stojkovski S., Sarkar B. (1993) Metal coordination to carbohydrates. Structures and function. Coord. Chem. Rev 122: 171-225

[6] (a) Cook W. J., Bugg C. E. (1973) A lactone-calcium chloride heptahydrate complex, Acta Cryst. B 29: 907-909; (b) Bugg C. E. (1973) Calcium binding to carbohydrates. Crystal structure of a hydrated calcium bromide complex of lactose. J. Am. Chem. Soc. 95: 908-913; (c) Cook W. J., Bug C. E. (1973) Calcium binding to galactose. Crystal structure of a hydrated α-galactose-calcium bromide complex. J. Am. Chem. Soc. 95: 6442-6446; (d) Cook W. J., Bugg C. E. (1973) Calcium interactions with d-glucans: crystal structure of α,α-Trehalose-calcium bromide monohydrate. Carbohydrate Res. 31: 265-275; (e) Ollis J., James V. J., Angyal S. J., Pojer P. M. (1978) An X-ray crystallographic study of α-d-allopyranosyl α-d-allopyranoside · $CaCl_2$ · $5H_2O$ (a pentadentate complex). Carbohydate Res. 60: 219-228; (f) Fujimoto T., Oku K., Tashiro M., Machinami T. (2006) Crystal Structure of α,α-Trehalose–Calcium Chloride Monohydrate Complex. J.Carbohydr. Chem. 25: 521-532; (g) Craig D. C., Stephenson M. C., Stevens J. D. (1974) Bis-(β-D-fructopyranose) calcium chloride trihydrate $2C_6H_{12}O_6 \cdot CaCl_2 \cdot 3H_2O$. Cryst. Struct. Commun. 3: 195-199; (h) Craig D. C., Stephenson M. C., Stevens J. D. (1974) Bis-(β-D-fructopyranose) calcium chloride dehydrate $C_6H_{12}O_6 \cdot CaCl_2 \cdot 2H_2O$. Cryst. Struct. Commun. 3: 277-281; (i) Cook W. J., Bugg C. E. (1976) Effects of calcium interactions on sugar conformation: crystal structure of β-D -fructose–calcium bromide dihyrate. Acta Cryst B 32: 656-659; (l) Guo J., Lu Y., Whiting R., Metal-Ion Interactions with Sugars. The Crystal Structure of CaCl2-Fructose Complex, Bull. Korean Chem. Soc., 2012, 33, 2028-2030; (m) J. Guo, X. Zhang (2004), Metal-ion interactions with sugars. The crystal structure and FTIR study of an $SrCl_2$ -fructose complex. Carbohydr. Res. 339: 1421-1426

[7] Oxford-Diffraction Ltd, Abingdon, UK

[8] CrysAlisPro, Agilent Technologies, Version 1.171.36.28

[9] SHELXTL, Version 5.1, Bruker AXS inc., Madison

[10] M. Sheldrick, SHELXL-2012

[11] Olex2 v. 1.2.4 @OlexSys Ltd. 2004-2013: Dolomanov O. V., Bourhis L. J., Gildea R. J., Howard J. A. K., Puschmann H. (2009) OLEX2: A complete structure solution, refinement and analysis program. J. Appl. Cryst. 42: 339-341

[12] Non-drying immersion oil for microscopy, type B, code 1248, Cargille Laboratories

[13] Enhance Ultra (Cu) X-ray Source, Agilent Technologies

[14] Mortati L., Divieto C., Sassi M. P. (2012) CARS and SHG microscopy to follow collagen production in living human corneal fibroblasts and mesenchymal stem cells in fibrin hydrogel 3D cultures. J. Raman Spectrosc. 43: 675–680

[15] Rasband W. S., Image J. (1997-2014) U. S. National Institutes of Health, Bethesda, Maryland, USA, http://imagej.nih.gov/ij/

[16] Gaussian 09, Revision A.02: Frisch M. J., Trucks G. W., Schlegel H. B., Scuseria G. E., Robb M. A., Cheeseman J. R., Scalmani G., Barone V., Mennucci B., Petersson G. A., Nakatsuji H., Caricato M., Li X., Hratchian H. P., Izmaylov A. F., Bloino J., Zheng G., Sonnenberg J. L., Hada M., Ehara M., Toyota K., Fukuda

R., Hasegawa J., Ishida M., Nakajima T., Honda Y., Kitao O., Nakai H., Vreven T., Montgomery J. A., Peralta J. E., Ogliaro F., Bearpark M., Heyd J. J., Brothers E., Kudin K. N., Staroverov V. N., Kobayashi R., Normand J., Raghavachari K., Rendell A., Burant J. C., Iyengar S. S., Tomasi J., Cossi M., Rega N., Millam J. M., Klene M., Knox J. E., Cross J. B., Bakken V., Adamo C., Jaramillo J., Gomperts R., Stratmann R. E., Yazyev O., Austin A. J., Cammi R., Pomelli C., Ochterski J. W., Martin R. L., Morokuma K., Zakrzewski V. G., Voth G. A., Salvador P., Dannenberg J. J., Dapprich S., Daniels A. D., Farkas Ö., Foresman J. B., Ortiz J. V., Cioslowski J., Fox D. J. (2009) Gaussian, Inc., Wallingford CT

[17] (a) Schlegel H. B., Csizmadia I. G., Daudel R., Reidel D. (1981) Publ Co, AB Initio Energy Derivatives Calculated Analytically. Computational Theoretical Organic Chemistry:129-159 ; (b) Schlegel H. B. (1982) An efficient algorithm for calculating a b i n i t i o energy gradients using s, p Cartesian Gaussians. J. Chem. Phys. 77: 3676-3681; (c) Schlegel H. B., Binkley J. S., Pople J. A. (1984) First and second derivatives of two electron integrals over Cartesian Gaussians using Rys polynomials. J. Chem. Phys. 80: 1976-1981; (d) Schlegel H. B. (1982) Optimization of equilibrium geometries and transition structures. J. Comput. Chem. 3: 214-218

[18] (a) Becke A. D. (1988) Density-functional exchange-energy approximation with correct asymptotic behaviour. Physical Review A 38: 3098–3100; (b) Becke A. D. (1993) Densityfunctional thermochemistry. III. The role of exact exchange. J. Chem. Phys. 98: 5648-5652; (c) Lee C., Yang W., Parr R. G. (1988) Development of the Colle-Salvetti correlation-energy formula into a functional of the electron density. Physical Review B 37: 785–789

[19] Hehre W. J., Radom L., Schleyer P. v R., Pople J. A. (1986) Ab initio Molecular Orbital Theory. Wiley, New York: 63-88.

[20] Parsons D. F., Ninham B. W. (2009) Ab Initio Molar Volumes and Gaussian Radii. J. Phys. Chem. A 113: 1141–1150

[21] Junicke H., Bruhn C., Kluge R., Serianni A. S., Steinborn D. (1999) Novel Platinum(IV)−Carbohydrate Complexes: Metal Ion Coordination Behavior of Monosaccharides in Organic Solvents. J. Am. Chem. Soc. 121: 6232-6241 and references therein.

[22] CSD-Cambridge Structural Database.

[23] Cochran W. (1946) Addition Compounds between Sucrose and the Sodium Halides. Nature 157: 231-231

[24] Tajmir-Riahi H. A. (1986) Sugar interaction with calcium ion. Synthesis and vibrational spectra of crystalline β-d-fructose and its calcium halide adducts. J. Inorg. Biochem. 27: 123-131

[25] Szarek W. A., Korppi-Tommola S. L., Shurvell H. F., Smith Jr. V. H., Martin O. R. (1984) A Raman and infrared study of crystalline D-fructose, L-sorbose, and related carbohydrates. Hydrogen bonding and sweetness. Can. J. Chem. 62: 1512-1518

[26] (a) Kanis D. R., Ratner M. A., Marks T. J. (1994) Design and Construction of Molecular Assemblies with Large Second-Order Optical Nonlinearities. Quantum Chemical Aspects. Chem. Rev. 94: 195-242; (b) Suponitsky K. Y., Tafur S., Masunov A. E. J. (2008) Applicability of hybrid density functional theory methods to calculation of molecular hyperpolarizability. J. Chem. Phys. 129 (044109): 1-11

[27] Bournill G., Mansour K., Perry K. J., Khundkar L., Sleva E. T., Kern R., Perry J. W. (1993) Powder second harmonic generation efficiencies of saccharide materials. Chem. Mater. 5: 802-808

Figure captions.

Fig. 1 Typical SHG spectrum emitted from the sample excited using the pulsed source tuned at a wavelength of about 915 nm

Fig. 2 Example of an obtained experimental curve of the overall average of 3D images at different excitation powers (triangles and yellow line) and the overlapped quadratic fitting solution

Fig. 3 XRPD patterns of solid mixtures of $CaCl_2$ and D-fructose in the stoichiometric ratio 3:1, 2:1, 1:1 and 1:2

Fig. 4 Coordination around the calcium ion and atom labelling (a) and the infinite network of calcium and chlorine ions and sugar molecules in the (001) plane (b) for compound **1**

Fig. 5 Coordination around the calcium ion and atom labelling (a) and the infinite network of calcium and chlorine ions and sugar molecules in the [010] direction (b) for compound **2**

Fig. 6 (a) Vibrational spectra (infrared-top, Raman-bottom) of D-fructose (black), compound **1** (red) and compound **2** (blue) from 3600 to 400 cm^{-1}; (b) detail of the same spectra from 3600 to 2700 cm^{-1}

Fig. 7 Conformations of fructose unit in D- fructose (a), compound **1** (b) and compound **2** (c)

Fig. 8 Plot of the logarithm of the SH intensity for compounds **1** (red), **2** (blue), sucrose (Su, green) and fructose (Fru, purple) versus $\omega/\omega_{\mathrm{exc}}$. The dots represent the ratio of the resonant frequency to the excitation frequency $\omega_0/\omega_{\mathrm{exc}}$

Fig. 9 Geometry, second-order susceptibility ($\mathrm{pm\ V^{-1}}$), and relative potential energy calculated at the B3LYP 6-31G(d) level of theory for Ca^{2+} $2Cl^-$ complexed by two molecules of fructose. Distances are in Å

Table 1. Ca-O bond lengths from X-ray data and B3LYP/6-31G(d) calculations

	XRD	B3LYP/ 6-31G(d)	XRD	B3LYP/ 6-31G(d)
	Compound **1**		Compound **2**	
Ca(1)-O(2)	2.355(2)	2.444	2.494(2)	2.506
Ca(1)-O(2A)[iii]				2.440
Ca(1)-O(3)	2.484(2)	2.563	2.462(2)	2.529
Ca(1)-O(3A)[iii]				2.557
Ca(1)-O(4)[i]	2.431(2)	2.416		
Ca(1)-O(5)[i]	2.437(2)	2.569		2.540
				2.517
Ca(1)-O(6)[ii]	2.372(2)	2.506		
Ca(1)-O(6B)[iv]			2.455(2)	2.433
Ca(1)-O(6C)[v]			2.455(2)	2.439
Ca(1)-O(1W)	2.349(2)	2.473	2.450(2)	
Ca(1)-O(2W)	2.323(2)	2.354		

Symmetry codes: (i) x+1, y, z; (ii) x+3/2, y-1/2, z+1; (iii) –x+2, y-2, z+2; (iv) x, y-1, z; (v) –x+2, y-1, z+2

Table 2. Fitting parameters a and b extracted from the experimental curves at different orientation angles per each analyzed sample, together with related average a per each angle and uncertainty due to the measurement repeatability.

Orientation Angles	Fit: *a*	Fit: *b*	Average *a* per Angle	*u(a*)
		Compound **1**		
0°	0.0207	-439	0.0235	0.0016
	0.0264	-767		
90°	0.0645	-2719	0.0632	0.0008
	0.0619	-2595		
180°	0.0356	-1195	0.0323	0.0019
	0.0290	-867		
270°	0.0200	-360	0.0215	0.0009
	0.0230	-579		
Average a	0.0351		Average *u(a)*	0.0016
		Compound **2**		
0°	0.0078	666	0.0068	0.0006
	0.0058	877		
90°	0.0060	704	0.0060	0.0001
	0.0061	719		
180°	0.0066	949	0.0077	0.0006
	0.0088	441		
270°	0.0064	603	0.0061	0.0001
	0.0059	573		
Average a	0.0067		Average *u(a)*	0.0004
		Sucrose		
0°	0.0139	-529	0.0146	0.0004
	0.0154	-630		
90°	0.0146	-558	0.0150	0.0002
	0.0153	-611		
180°	0.0183	-840	0.0184	0.0001
	0.0186	-856		
270°	0.0123	-472	0.0122	0.0001
	0.0121	-461		
Average a	0.0151		Average *u(a)*	0.0002

Table 3. Ratio of the SHG intensity measured for the two compounds with respect to the sucrose with their uncertainty related to the measurement repeatability.

Structure	I/I_{sucr}
Compound **1**	2.33 ± 0.11
Compound **2**	0.44 ± 0.02

Table 4. Theoretical computed ground state optimized parameters: dipole moment μ (Debye), mean polarizability <α> (a.u.) and all β components (a.u.) calculated for compounds 1, 2, fructose and sucrose.

	Compound 1	Compound 2	Fructose	Sucrose
μ	38.54	28.91	2.14	9.03
<α>	672.2	671.1	591.7	484.5
β_{xxx}	210.36	-643.07	16.36	256.94
β_{xxy}	68.60	-180.87	-9.65	-89.34
β_{xyy}	138.10	-190.80	8.75	136.22
β_{yyy}	541.12	-319.98	117.50	-365.37
β_{xxz}	143.70	316.18	9.98	-23.24
β_{xyz}	1.25	75.66	14.06	-60.95
β_{yyz}	309.45	171.13	34.70	19.35
β_{xzz}	-67.65	-222.11	0.74	73.92
β_{yzz}	101.64	-178.52	1.00	-68.58
β_{zzz}	1113.30	346.02	-81.65	-183.54

Table 5. Resonant angular frequency ($\omega_0/10^{15}\ \mathrm{rad\ s^{-1}}$), hyperpolarizability ($\beta_{\mathrm{tot}}/10^{-30}\ \mathrm{cm^5\ esu^{-1}}$), second-order susceptibility ($\chi^{(2)}/\mathrm{pm\ V^{-1}}$), and ratio of SH intensities with respect to sucrose calculated at the B3LYP 6-31G(d) level of theory and $\gamma = 4.123 \times 10^{15}\ \mathrm{rad\ s^{-1}}$ for fructose, sucrose and compounds **1** and **2**.

Structure	ω_0	β_{tot}	$\chi^{(2)}$	I/I_{sucr}
Fructose	11.59	1.34	0.32	0.11
Sucrose	10.33	6.27	1.82	1.00
Compound **1**	6.334	15.06	3.03	2.33
Compound **2**	7.199	13.02	2.64	0.61

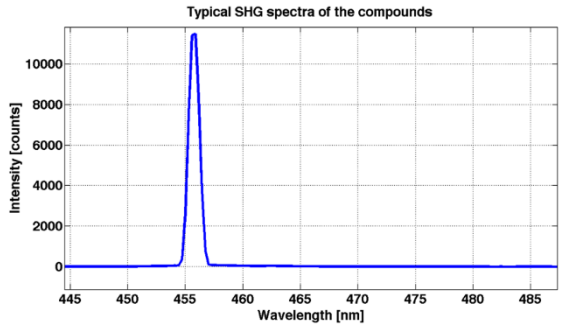

Figure 1

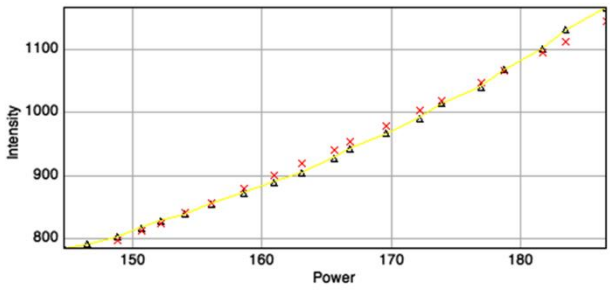

Figure 2

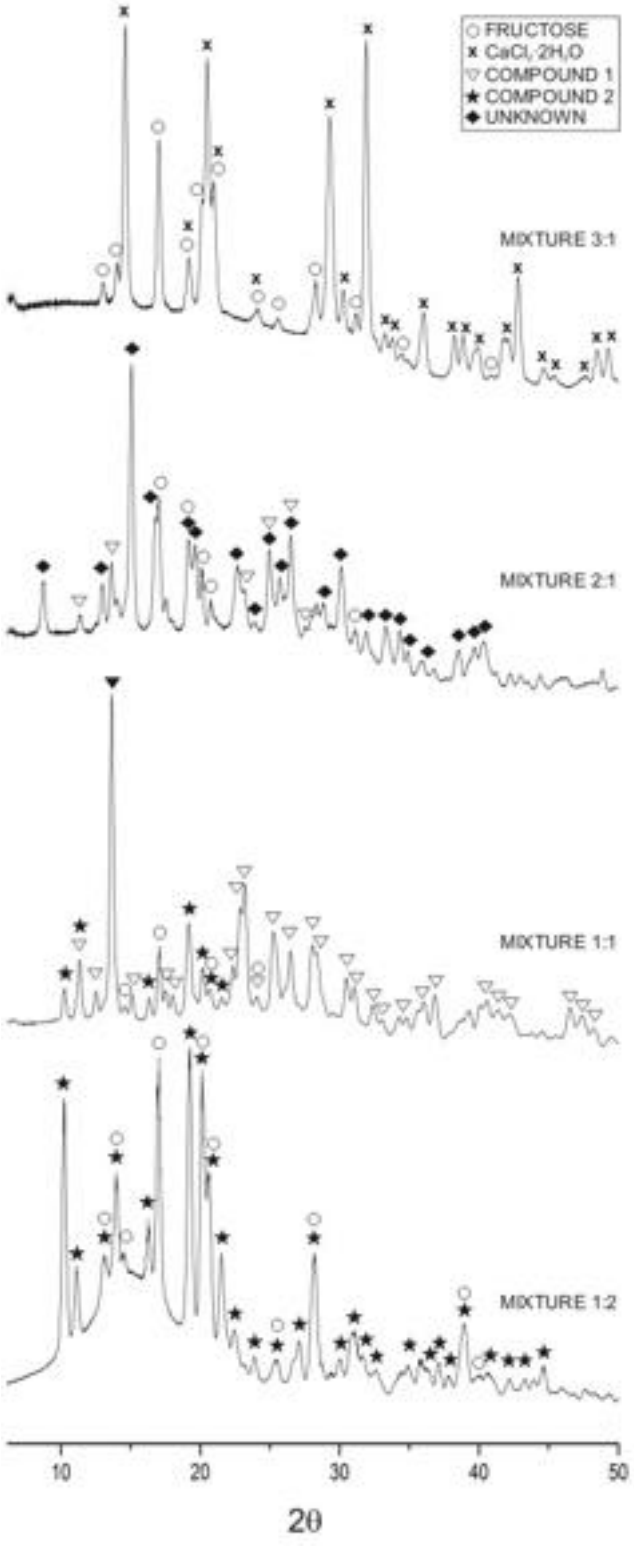
FRUCTOSE
CaCl2.2H2O
COMPOUND 1
COMPOUND 2
UNKNOWN
MIXTURE 3:1
MIXTURE 2:1
MIXTURE 1:1
MIXTURE 1:2
10
20
30
40
50
2θ

Figure 3

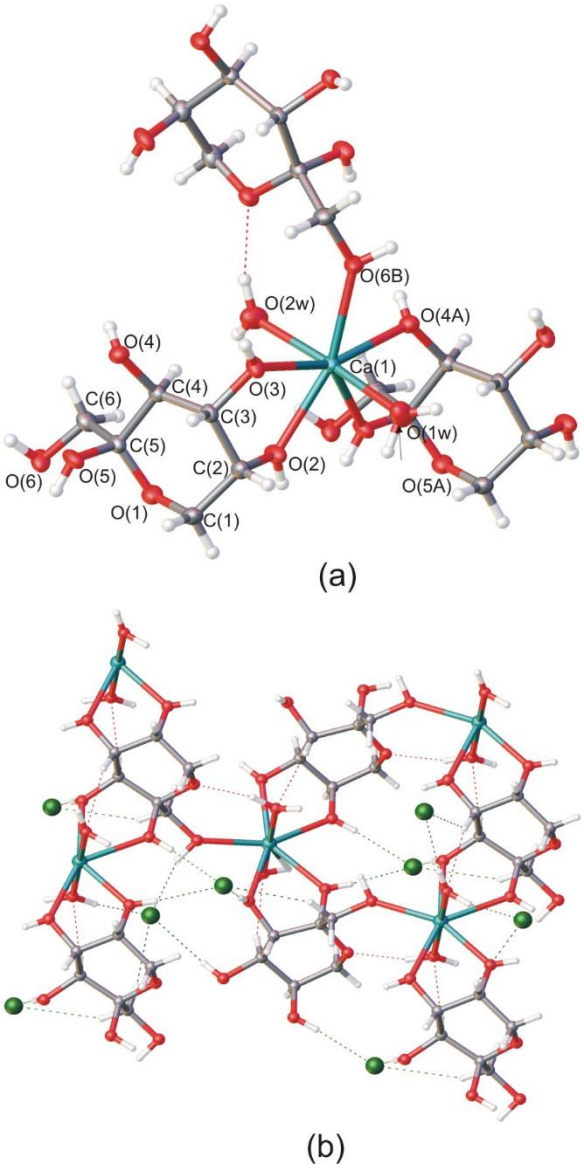

Figure 4

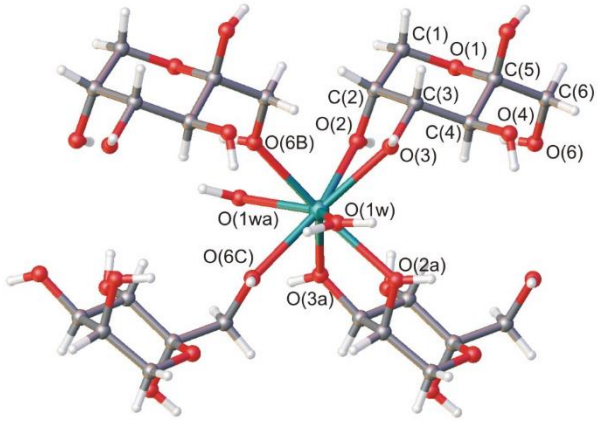

(a)

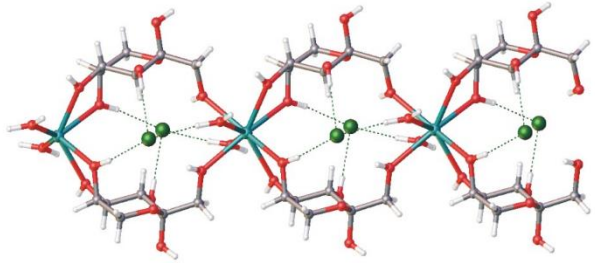

(b)

Figure 5

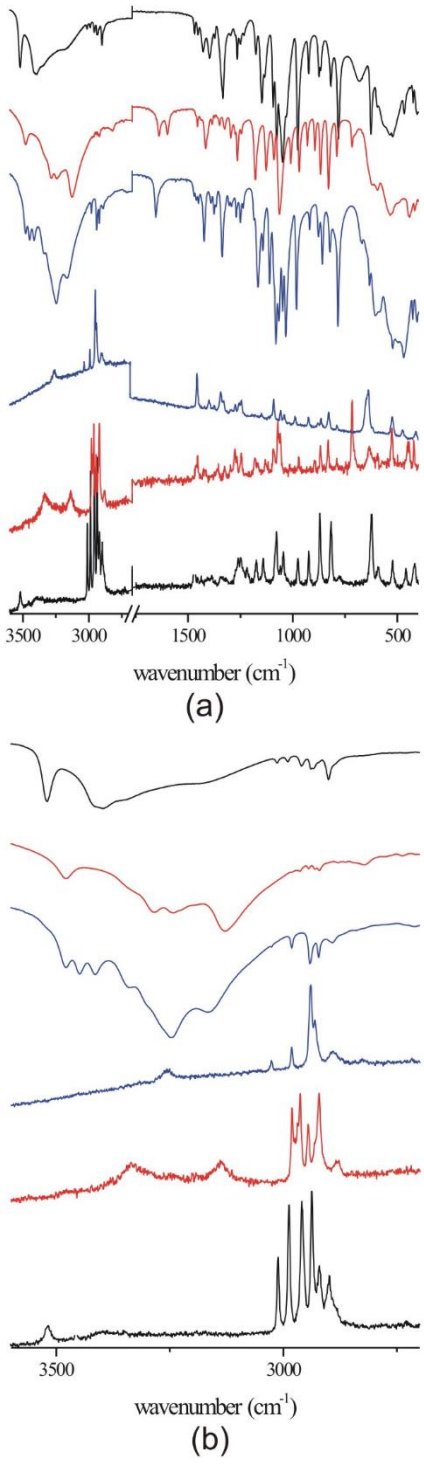
3500
3000
1500
1000
500
wavenumber (cm-1)
(a)
3500
3000
wavenumber (cm-1)
(b)

Figure 6

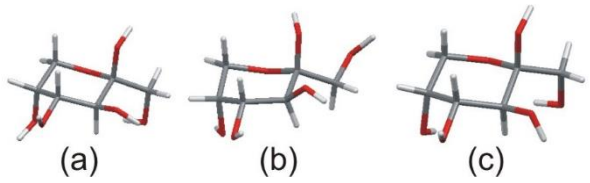

Figure 7

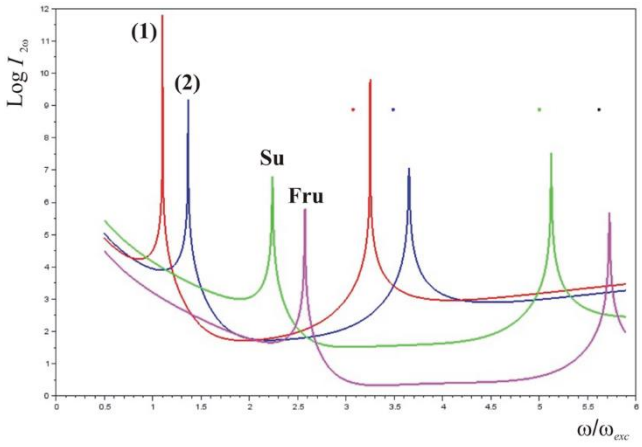

Figure 8

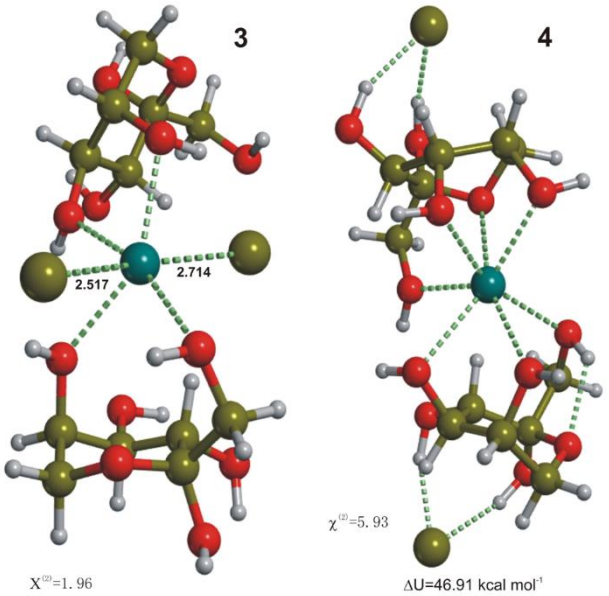

Figure 9

SUPPLEMENTARY MATERIALS

Article title: Non Linear Optical Properties of β-D-Fructopyranose Calcium Chloride MOFs: an Experimental and Theoretical Approach

Journal: Journal of Materials Science

Authors: DOMENICA MARABELLO* [a,b], PAOLA ANTONIOTTI[a], PAOLA BENZI[a,b], CARLO CANEPA[a], ELIANO DIANA[a,b], LORENZA OPERTI[a,b], LEONARDO MORTATI[c], MARIA PAOLA SASSI[c]
[a] *Dipartimento di Chimica, University of Torino, Italy*
[b] *CrisDi-Interdepartmental Center for Crystallography, University of Torino, Italy*
[c] *INRIM – Istituto Nazionale di Ricerca Metrologica, Italy*
E-mail: domenica.marabello@unito.it, +390116707505

Table 1s. Details on crystal data, data collection and refinement.

	*Compound **1***	*Compound **2***
Formula	$CaC_6H_{16}O_8Cl_2$	$CaC_{12}H_{34}O_{15}Cl_2$
Formula weight	327.17	529.37
Crystal size (mm)	0.21x0.10x0.07	0.33x0.09x0.09
Crystal color, shape	Colorless, prismatic	Colorless, prismatic
Crystal system	monoclinic	monoclinic
Space group	$P2_1$	C2
a (Å)	7.0731(2)	16.016(1)
b (Å)	11.7023(3)	7.8393(2)
c (Å)	7.7808(3)	9.2442(3)
β (°)	93.998(3)	98.601(3)
V (Å^3), Z	642.46(3), 2	684.40(4), 2
Dcalc (g cm^{-3})	1.691	1.631
μ (cm^{-1})	0.929	0.611
Min/max transmission	0.860/0.948	0.914/0.964
Scan mode	ω	ω
θ range	3.372-32.773	3.208-32.698
Index ranges	-10≤h≤10	-23≤h≤22
	-16≤k≤14	-11≤k≤11
	-11≤l≤11	-15≤l≤16
Collected reflections	7220	5988
Independent reflections	3460	3428
R_{int}	0.0296	0.0245
Parameters number	163	152
Observed reflections (I≥2σ(I))	3150	3018
R1, wR2	0.0335, 0.0711	0.0375, 0.0734
GooF	1.041	1.032
Largest peak and hole (eÅ^{-3})	0.283, -0.291	0.341, -0.263
Max shift/e.s.d	< 0.001	< 0.001

Table 2s. Infrared and Raman vibrational frequencies of compounds 1 and 2.

D-fructose		Compound **1**		Compound **2**	
IR	Raman	IR	Raman	IR	Raman
3517 s	3517 m	3481m	3481w	3480 m	
3406 s	3406 br m-w	3338 m sh	3338 br	3449 m	
3180 br		3288 br m		3414 m	
3012 w	3012 s	3243 br m	3243 br w	3344 sh m	
2991 w	2988 vs	3130 s	3137 m	3251 vs	3251 m
2960 mw	2960 vs	2981 vw	2981 s	3162 s	
2938 m	2938 vs		2975 m	3027 vvw	3027 w
	2921 s	2969 vvw	2969 s	2981 w	2981 m
2901 m	2901 s	2963 wv	2963 vs	2940 m	2940 vs
1471 w	1471 s	2945 vw	2945 s		2931 s
1452 w	1452 w	2930 vw	2930 m	2922 m-w	2922 sh
1430 m		2921 vw	2921 vs	2891 vw	2891 br m
1399 m		2880 vw	2880 w	1655 m	
1373 w		1638 m		1471 w	
1335 s	1335 w	1599 m		1461 w	
1298 w		1455 m	1455 m	1449 w	1449 s
1265 m	1265 m	1417 s	1417 w	1424 m	
1250 mw	1250 m	1386 w		1391 w	1391 w
1233 w			1356 m	1376 w	
1217 m	1217 m	1350 w		1367 w	1367 w
1175 m	1175 m	1325 w	1325 m	1337 m-s	1337 m
1148 s		1298 m	1298 m	1323 sh	1323 m
1136 m	1136 m	1276 w	1276 m-s	1304 w	
1095 s	1095 s	1264 s	1264 m	1291 w	
1077 vs	1077 s	1246 w	1246 m	1270 w	1270 m
1048 vs	1048 m	1178 s	1178 m	1251 m	1251 m
1031 sh		1129 s	1129 m	1239 w	1239 w
977 vs	977 m	1092 m	1092 s	1185 sh	
924 m	924 m	1072 sh	1072 s	1166 s	
874 m		1065 vs	1065 m	1143 m	1143 vw
869 m	869 s	1053 sh	1053 s	1110 s	1110 vw
818 m	818 s	1010 m	1010 w	1091 sh	1086 sh
781 vs	781 w	970 s	970 m	1080 vs	
683 br		930 m		1066 s	
626 s	626 s	895 m	895 m		1054 m
592 m	592 w	867 s	867 m	1048 s	
562 sh		830 vs	830 s	1035 vs	1035 m-w
538 s		790 m	790 w	963 s	963 w
522 s	522 m	717 m	717 vs	920 w	920 w
466 m		637 sh s	637 br m	875 w	875 vw
	460 m	621 s		860 m	860 w
427 m	427 m	595 s	595 m	825 m	825 m
404 m		540 s	540 br	784 vs	784 vw
		525 sh s	525 s	674 sh	674 m
		450 sh m	450 m	634 m	634 vs
		445 m	445 m	608 s	
			422 m	525 m	525 m
		416 w		472 m	472 w
		393w		427 w	
				409 w	409 w

Figure 1s. XRPD patterns for compounds **1** (a) and **2** (b) compared respectively with those calculated from single crystal x-ray structures of FRUCCA and FRCPCA obtained from CSD database. The patterns were reported only in the range of $2\theta = 9 \div 50$ where the more significant features are observed.

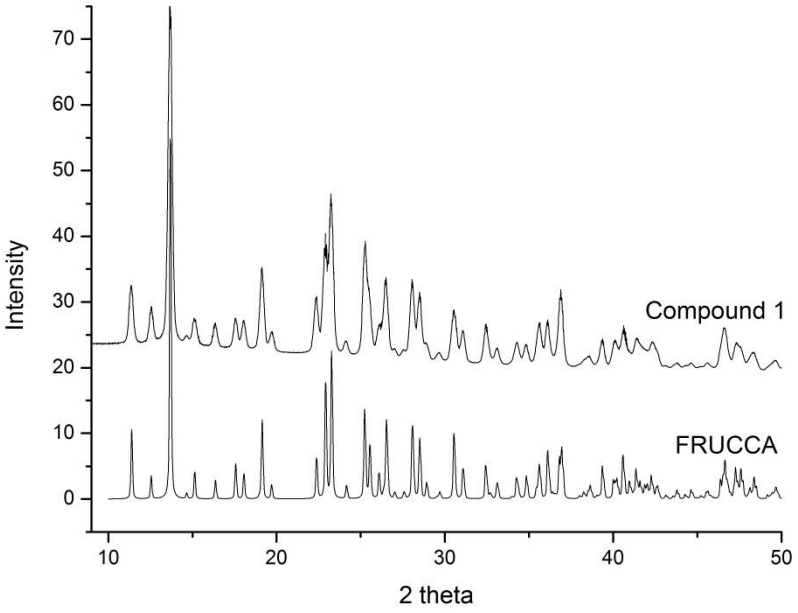

(a)

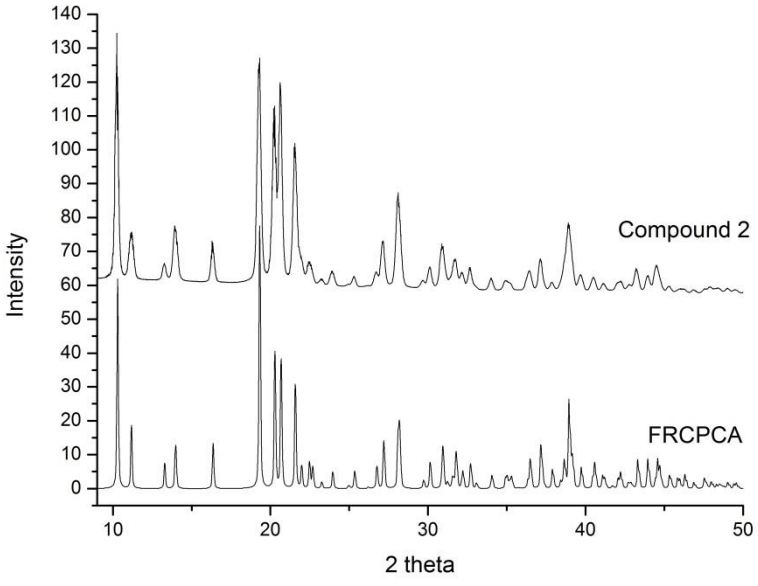

(b)